Journal of Physics: Conference Series **137** (2008) 012005 doi:10.1088/1742-6596/137/1/012005

# Bifurcation behavior of standing waves

**J. Abshagen, M. Heise, J. Langenberg, and G. Pfister**

Institute of Experimental and Applied Physics, University of Kiel, 24098 Kiel, Germany

E-mail: abshagen@physik.uni-kiel.de

**Abstract.** Two different types of standing waves ($\mathrm{SW}_0$ and $\mathrm{SW}_\pi$) can appear instead of spiral vortices from a supercritical Hopf bifurcation in counter-rotating Taylor-Couette flow for sufficiently small aspect ratios [1,2]. The bifurcation sequence from basic flow to spiral vortices via $\mathrm{SW}_0$ can include modulated waves, homoclinic bifurcations, and hysteresis as a consequence of broken translational invariance [3]. Here we show that the same kind of sequence can also occur for the other type of standing wave, i.e., $\mathrm{SW}_\pi$. Furthermore we show that $\mathrm{SW}_\pi$ can exist also up to much larger inner Reynolds numbers than is has been found for $\mathrm{SW}_0$. Far from onset $\mathrm{SW}_\pi$ can undergo bifurcation sequences that differs qualitatively from those close to onset. These sequences involve a supercritical symmetry breaking as well as a supercritical Hopf bifurcation towards a new type of modulated wave.

## 1. Introduction

Spiral vortices can appear from linear instability of circular Couette flow (CCF) in the annulus between two rotating cylinders [4–6]. CCF is the basic laminar flow of the Taylor-Couette system, one of the classical hydrodynamic systems for the study of bifurcation events [7–9]. It is invariant under axial translations and reflection and under azimuthal rotation, i.e., invariant under the group $O(2) \times SO(2)$ [6,10]. Spiral vortices are traveling waves in axial and rotating waves in azimuthal direction which break these symmetries (they have an azimuthal wave number $m = \pm 1$ for the parameter values considered here). Their bifurcation behavior from CCF can be understood from a Hopf bifurcation with $O(2)$ symmetry [5,6,10,11].

Spiral vortices have been first calculated theoretically by Krueger *et al.* [12] and observed experimentally by Snyder [13]. Subsequent experimental and numerical studies on spiral vortices have been carried out by Andereck *et al.* [14], Langford *et al.* [11] as well as Sanchez *et al.* [15] and Hoffmann *et al.* [16], respectively, in a wide Reynolds number regime for different radius and aspect ratios.

Non-rotating rigid end plates at top and bottom as often used in experimental systems change the properties of spirals in counter-rotating Taylor-Couette flow due to the presence of rotating defects in the vicinity of the axisymmetric Ekman vortices near the end plates [16]. As a consequence of broken translational invariance in experimental systems two different types of standing waves (denoted $\mathrm{SW}_0$ and $\mathrm{SW}_\pi$) are found to replace spiral vortices as the primary pattern that occur from a supercritical Hopf bifurcation of the basic laminar flow [1,2]. This has been predicted theoretically by Dangelmayr and Knobloch [17] and Landsberg and Knobloch [18] in a theory of Hopf bifurcation with broken translational invariance. Both types differ in the kind of reflection symmetry, i.e., $\mathrm{SW}_0$ has a spatial while $\mathrm{SW}_\pi$ has a spatio-temporal glide reflection symmetry.

 

The theoretically predicted bifurcation sequence involves secondary steady super- or subcritical bifurcations towards spiral vortices as well as more complex bifurcation sequences involving a secondary Hopf bifurcation towards modulated waves, homoclinic bifurcations, a Takens-Bogdanov point, and hysteresis. While the former part has been observed in experiments for both types of standing waves, i.e., $\mathrm{SW}_0$ and $\mathrm{SW}_\pi$ [1, 2], the latter point has only been investigated for $\mathrm{SW}_0$ [3]. In this work we focus on higher bifurcations from the other type of standing wave in counter-rotating Taylor-Couette flow, i.e., $\mathrm{SW}_\pi$.

## 2. Experimental setup

A Taylor-Couette apparatus with counter-rotating cylinders and non-rotating end plates is used for this study, as described in [1–3]. The inner cylinder of the apparatus is machined from stainless steel having a radius of $r_i = (12.50 \pm 0.01)$ mm, while the outer cylinder is made from optically polished glass with a radius of $r_o = (25.00 \pm 0.01)$ mm. The flow is confined in the axial direction by non-rotating end plates at top and bottom separated by a distance $L$ which defines the axial length of the system. Geometric parameters of the system are the aspect ratio $\Gamma = L/d$, with gap width $d = r_o - r_i$, and the radius ratio $\eta = r_i/r_o = 0.5$. The Reynolds number of the inner ($i$) and the outer ($o$) cylinder serve as control parameters $Re_{i,o} = dr_{i,o}\Omega_{i,o}/\nu$, where $\Omega_{i,o}$ denotes the angular velocity of the inner ($i$) and the outer ($o$) cylinder, respectively. Thermostatically controlled silicone oil ($(24.00 \pm 0.01)$°C) is used as a working fluid with a kinematic viscosity $\nu = 10.8$ cSt. Spatial and temporal properties of the velocity field are determined by local measurements of a axial velocity using Laser-Doppler velocimeter (LDV). The LDV measurement volume has a distance of 1.5 mm from the inner cylinder and is either located at a fixed axial position or moves at constant speed along a path $z(t)$ in axial direction during the measurements. The latter procedure yields an axial scan which allows a spatio-temporal characterization of stationary flow states.

## 3. Results

### *3.1. $SW_\pi$ close to onset*

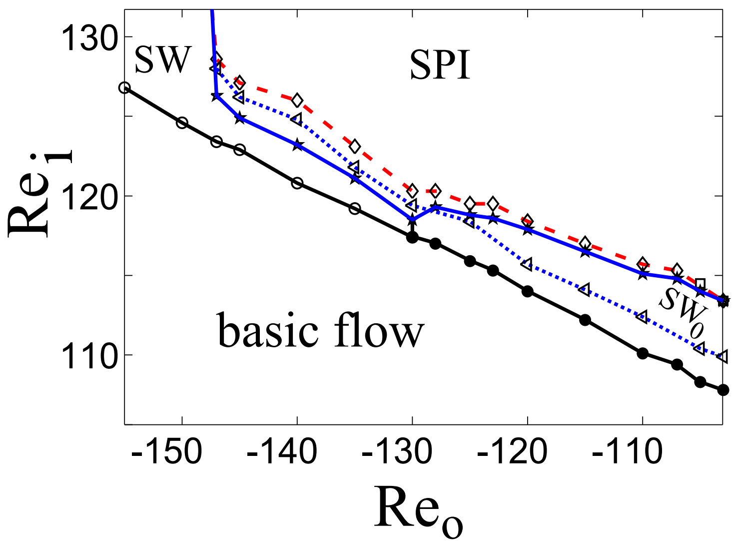


**Figure 1.** Stability diagram of counter-rotating Taylor-Couette flow for $\Gamma = 7.3$: Transition from basic flow to spiral vortices SPI ($\diamond$, red dashed line) close to onset via a sequence of standing waves $\mathrm{SW}_0$ ($\bullet$) or $\mathrm{SW}_\pi$ ($\circ$) and modulated waves ($\star$, blue solid line) – hysteresis regime of SPI is marked by ($\triangle$, blue dashed line).

$SW_0$ appears from basic flow instead of spiral vortices from a supercritical Hopf bifurcation as a consequence of linear instability of the basic laminar flow. Spiral vortices can occur from $SW_0$ at slightly higher $Re_i$ directly from a super- or subcritical symmetry breaking bifurcation. However, a more complex bifurcation sequence of $SW_0$ can occur involving a secondary Hopf bifurcation to modulated waves and a homoclinic bifurcation both resulting from a Takens-Bogdanov point [3, 17, 18]. The latter scenario is depicted in figure 1 for $SW_0$ ($\bullet$) but it also occurs for $SW_\pi$ ($\circ$) close to onset (here aspect ratio is $\Gamma = 7.3$). Modulated wave ($\star$) appear from both types of SW and the flow undergoes a homoclinic bifurcation ($\diamond$) towards spiral vortices at higher $Re_i$. The hysteresis regime of spiral vortices is marked by ($\triangle$). Note, that the transition between $SW_0$ and $SW_\pi$ involves a cusp point which is not resolved in figure 1 [1]. It can be seen that qualitatively the same bifurcation scenario can be found for $SW_\pi$ close to onset as it has been studied in detail for $SW_0$ in [3]. Here the entire transition from basic flow to spirals occurs within a few $Re_i$. However, there are parameter regimes where $SW_\pi$ is found to be stable up to much larger Reynolds numbers. Such a regime is indicated for $\Gamma = 7.3$ in figure 1 at $Re_o \lesssim -147$.

*3.2. SWπ far from onset*

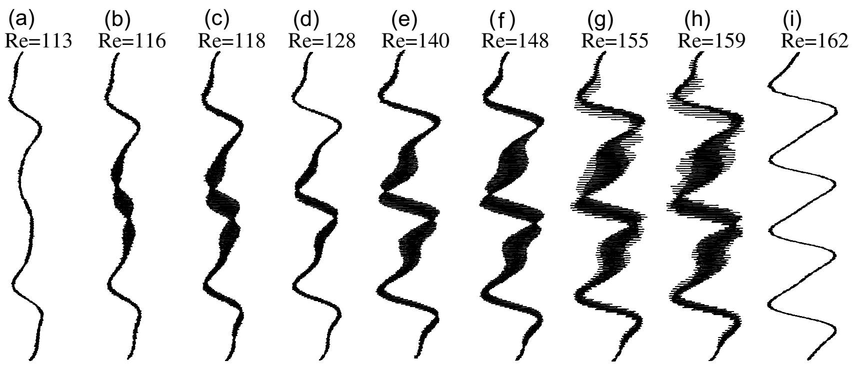


**Figure 2.** Axial scans of (a) basic flow ($Re_i = 113$), (b,c,d,e) $SW_\pi$ ($Re_i = 116, 118, 128, 140$), (f) asymmetric $SW_\pi$ ($Re_i = 148$), (g) modulated $SW_\pi$ ($Re_i = 155$), (h) chaotic flow ($Re_i = 159$), and (i) Taylor vortex flow ($Re_i = 162$) recorded at $Re_o = -125$ and $\Gamma = 5.7$.

An axial scan of the basic laminar flow and $SW_\pi$ at sub- and slightly supercritical $Re_i$ are shown in figure 2(a) and (b), respectively. They are recorded at $Re_o = -125$ and $\Gamma = 5.7$. For this aspect ratio $\Gamma$ a large regime of stable $SW_\pi$ is found. The sequence of axial scans of $SW_\pi$ depicted in figure 2(b)-(e) indicates such a large regime at $Re_i = 116 \ldots 140$. Note that the amplitude of $SW_\pi$ does not increase monotonically with $Re_i$ and has a local minimum at about $Re_i = 128$, corresponding to the axial scan in figure 2(d). It will be shown in the following that this behavior is due to the stability properties of $SW_\pi$ at $\Gamma = 5.7$ (see discussion of stability diagram in figure 3 below). The spatio-temporal reflection symmetry of $SW_\pi$ is broken at higher $Re_i$ and an asymmetric $SW_\pi$ state appears. Such a flow state is recorded at $Re_i = 148$ and is plotted in figure 2(f). In figure 2(g) an axial scan of an asymmetric modulated $SW_\pi$ is depicted ($Re_i = 155$). This flow state becomes chaotic at higher Reynolds number (see figure 2(h) for axial scan at $Re_i = 159$) and finally undergoes a hysteretic transition to steady Taylor vortex flow ($Re_i = 162$, figure 2(i)) towards higher $Re_i$.

The axial scans depicted in figure 2 are all recorded at $Re_o = -125$. The dependence of this sequence on $Re_o$ can be seen from the stability diagram shown in figure 3. The Reynolds numbers corresponding to the flow states from figure 2 are marked in figure 3 along the vertical dashed line at $Re_o = -125$. The supercritical Hopf bifurcation curve from basic laminar flow to $SW_\pi$ (green curve) exhibits a notch at $Re_i \approx 130$. This notch is responsible for the reduction in amplitude observed in the sequence in figure 2(c)-(e) for $Re_o = -125$ since the distance from the vertical path with fixed $Re_o$ to the Hopf bifurcation curve shrinks again due to the notch. However, between $Re_o \approx -140 \ldots -120$ stable $SW_\pi$ exists for about $\Delta Re_i \approx 40$. This regime is larger than that found for $SW_0$ in [1–3]. For outer Reynolds numbers $Re_o \geq -100$ a continuous transition to Taylor vortex flow (TVF) occurs since the bifurcation is destroyed due to the presence of rigid end plates at top and bottom.

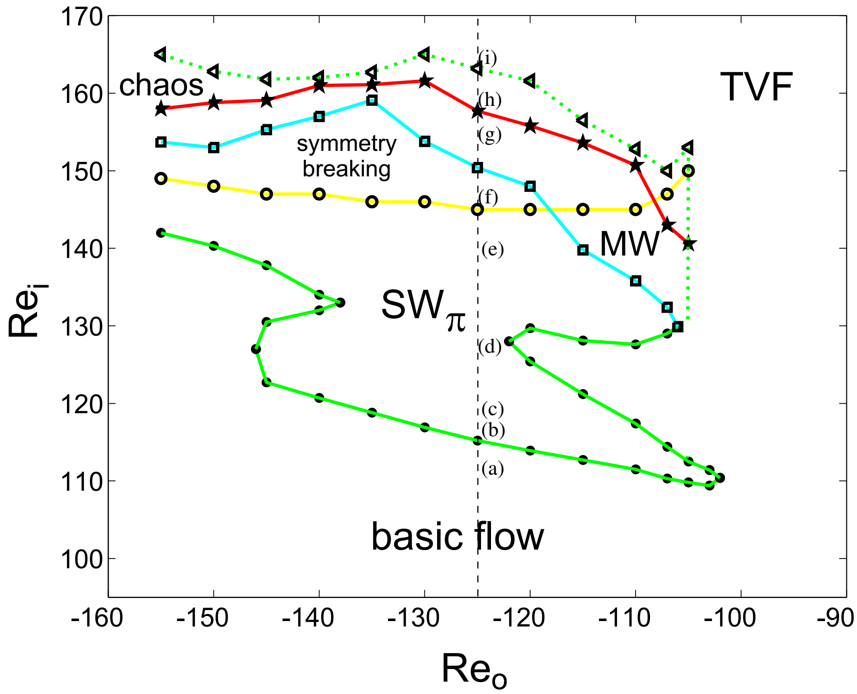


**Figure 3.** Stability diagram at $\Gamma = 5.7$: ($\bullet$, green line) Hopf bifurcation to $SW_\pi$, ($\circ$, yellow line) breaking of reflection symmetry, ($\square$, blue line) onset of modulation, ($\star$, red line) onset of chaos, and ($\triangle$, dashed green line) hysteretic transition to Taylor vortex flow. The labels along the vertical dashed line at $Re_0 = -125$ mark the Reynolds numbers of the corresponding flow states shown in figure 2.

The standing wave $SW_\pi$ breaks its spatio-temporal reflection symmetry slightly below $Re_i \approx 150$ as indicated by the yellow curve in figure 3, via a supercritical asymmetric bifurcation. Furthermore a modulation appears from a second Hopf bifurcation which is marked by a blue curve in figure 3. Axial scans of these flow states are shown in figure 2 (f) and (g), respectively. The Hopf and symmetry-breaking bifurcation curves can cross at a certain $Re_o$ and the modulation can occur either at lower or higher $Re_i$ than the symmetry breaking, depending on $Re_o$. The modulated symmetric and asymmetric SW can become chaotic at higher $Re_i$ (red curve in figure 3) and finally undergoes a hysteretic transition to Taylor vortex flow with eight cells at the dashed green curve in figure 3. This bifurcation sequence differs substantially from those found close to onset for both $SW_0$ and $SW_\pi$. At onset the reflection symmetry is either broken by a super- or a subcritical bifurcation. The subcritical bifurcation is part of a Takens-Bogdanov scenario which can include also a supercritical Hopf bifurcation towards modulated waves. Away from onset, a supercritical symmetry breaking can appear together with a supercritical Hopf bifurcation toward modulated waves.

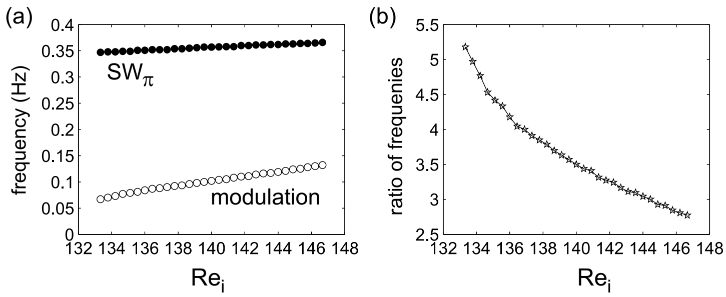


**Figure 4.** (a) Oscillation frequencies of $\mathrm{SW}_\pi$ (•) and modulations (◦) versus $Re_i$ at $\Gamma = 5.7$ and $Re_o = -107$, (b) frequency ratio versus $Re_i$.

A typical dependence of the modulation frequency on $Re_i$ is depicted in figure 4(a) for $Re_o = -107$, i.e., in the regime of symmetric modulated $\mathrm{SW}_\pi$. The modulation frequency is around $f_{mod} \approx 0.1$ Hz in our experiments and therefore a factor of 2.5 to 5 smaller than the frequency of SW. The latter have a frequency of about $f_{SW_\pi} \approx 0.35$ Hz which is typical for the experimental configuration used here (see e.g., [1]). The exact frequency ratio is given in figure 4(b). The ratio decreases since the modulation frequency increases with $Re_i$ while the frequency of SW is almost constant with $Re_i$. The frequency of the modulation that appears further away from onset is therefore an order of magnitude larger than the one close to onset [3].

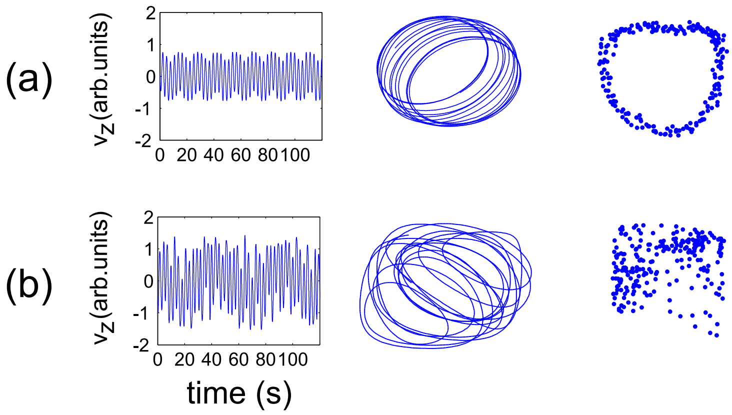


**Figure 5.** Time series (left), phase space reconstruction (middle), and Poincaré section (right) of typical flow states in the regime of symmetric modulated SW at $\Gamma = 5.7$ and $Re_o = -107$: (a) quasi periodic flow at $Re_i = 134.1$, (b) chaotic flow at $Re_i = 146.7$.

Dynamical characteristics, such as time series, phase space reconstruction, and Poincaré sections, of the modulated SW recorded in the (a) quasi periodic and in the (b) chaotic regime are depicted in figure 5. The flow in the quasi periodic regime, such as that represented in (a) for $Re_i = 134.1$, evolves on a $T^2$-torus. Since the ratio of frequencies decreases with $Re_i$, as indicated in figure 4(b), also commensurable ratios of frequencies must exist for certain $Re_i$. Such flow states are indeed observed, e.g., for $\frac{f_{SW_\pi}}{f_{mod}} = \frac{4}{1}, \frac{7}{2}, \frac{3}{1}$ at $Re_i = 136.9, 140.0, 144.4$, where the flow forms a limit cycle. However, within a resolution of $\Delta Re_i = 0.1$, there is no clear evidence that both frequencies lock at these ratios since no plateau is found (see figure 4(b)). At higher $Re_i$, e.g., $Re_i = 146.7$, the $T^2$-torus breaks up and a chaotic state appears. Characteristics of this flow are shown in figure 5(b). Since only peaks related to the two modes are found in the power spectrum there is no evidence for a further mode but for nonlinear coupling of these two modes.

## 4. Conclusions

We have experimentally investigated the bifurcation behavior of one type of standing wave $SW_\pi$ that appears instead of spiral vortices in counter rotating Taylor-Couette flow for sufficiently small aspect ratios. In previous studies [1, 2] the appearance and the primary bifurcation of $SW_\pi$ and of another type of standing wave, i.e., $SW_0$, have been investigated. Both types of standing waves appear in principle instead of spiral vortices as a consequence of broken translational invariance of the experimental system [17, 18]. More complex bifurcation behavior in the sequence from basic flow to spiral vortex flow including modulated standing waves, homoclinic bifurcations, and hysteresis has been found for $SW_0$ [3]. This has also been predicted from bifurcation theory [17, 18]. In this work we have presented experimental results that reveal the same bifurcation sequence to appear for $SW_\pi$, close to onset. Therefore the theoretically predicted bifurcation sequence is not limited to one type of standing wave in the experiment but is generally applicable to both types of SW.

Furthermore we found that $SW_\pi$ can be stable in some parameter regimes up to much larger $Re_i$. While the transition from basic flow to spiral vortex flow typically occurs within a few $Re_i$ (see [2, 3]) a stability interval of several tens of $Re_i$ could be found for $SW_\pi$. Further away from onset we found a supercritical symmetry breaking bifurcation as it is also observed close to onset but additionally we found a new type of modulated standing wave. This state originates from another supercritical Hopf bifurcation for both symmetric and asymmetric $SW_\pi$ with a frequency of an order of magnitude larger than the modulation found close to onset [3]. Therefore the bifurcation behavior of $SW_\pi$ far from onset can substantially differ from the one close to onset.

## Acknowledgments

We acknowledge support from the Deutsche Forschungsgemeinschaft.

## 5. References

[1] Langenberg J, Pfister G and Abshagen J 2003 *Phys. Rev. E* **68** 056308
[2] Langenberg J, Pfister G and Abshagen J 2004 *Phys. Fluids* **16** 2757–2762
[3] Langenberg J, Pfister G and Abshagen J 2004 *Phys. Rev. E* **70** 046209
[4] Egbers C and Pfister G 2000 *Physics of rotating fluids* (Springer Verlag, Berlin)
[5] Golubitsky M Stewart I and Schaeffer D G 1988 *Singularities and Groups in Bifurcation Theory* vol 2 (Applied Mathematical Sciences, Springer-Verlag)
[6] Chossat P and Iooss G 1994 *The Couette-Taylor Problem* (Springer-Verlag)
[7] diPrima R and Swinney H 1981 *Hydrodynamic instabilities and the transition to turbulence* ed Swinney H and Gollub J (Springer, Berlin) pp 139–180
[8] Tagg R 1994 *Nonlinear Science Today* **4** 1–25
[9] Cross M C and Hohenberg P C 1993 *Rev. Mod. Phys.* **65** 851
[10] Golubitsky M and Stewart I 1986 *SIAM Journal of Mathematical Analysis* **17** 249
[11] Langford W F, Tagg R, Koesterlich E J, Swinney H L and Golubitsky M 1988 *Phys. Fluids* **31** 776–785
[12] Krueger E R, Gross A and di Prima R C 1966 *J. Fluid Mech.* **24** 521
[13] Snyder H A 1968 *Phys. Fluids* **11** 728–734
[14] Andereck C D, Lui S S and Swinney H L 1986 *J. Fluid Mech.* **164** 155–183
[15] Sanchez J, Crespo D and Marques F 1993 *Appl. Sci. Res.* **51** 55–59
[16] Hoffmann C, Lücke M and Pinter A 2005 *Phys. Rev. E* **72** 056311
[17] Dangelmayr G and Knobloch E 1991 *Nonlinearity* **4** 399–427
[18] Landsberg A S and Knobloch E 1996 *Phys. Rev. E* **53** 3579–3600